Liquid Crystals
Publication details, including instructions for authors and subscription information:
http://www.informaworld.com/smpp/title~content=t713926090

X-ray and calorimetric study of smectic -smectic A_2-smectic C_2 transitions in a liquid crystal mixture

L. Wu[a]; C. W. Garland[a]; S. Somasekhar[b]; R. Shashidhar[c]
[a] Center for Materials Science and Engineering and Department of Chemistry, Massachusetts Institute of Technology, Cambridge, Massachusetts, U.S.A. [b] Raman Research Institute, Bangalore, India [c] Center for Bio/Molecular Science and Engineering, Code 6090, Naval Research Laboratory, Washington, D.C., U.S.A.

To cite this Article Wu, L. , Garland, C. W. , Somasekhar, S. and Shashidhar, R.(1993) 'X-ray and calorimetric study of smectic -smectic A_2-smectic C_2 transitions in a liquid crystal mixture', Liquid Crystals, 13: 4, 507 — 514
To link to this Article: DOI: 10.1080/02678299308026323
URL: http://dx.doi.org/10.1080/02678299308026323

LIQUID CRYSTALS, 1993, VOL. 13, NO. 4, 507–514

X-ray and calorimetric study of smectic C̃–smectic A_2–smectic C_2 transitions in a liquid crystal mixture

by L. WU and C. W. GARLAND*
Center for Materials Science and Engineering and Department of Chemistry, Massachusetts Institute of Technology, Cambridge, Massachusetts 02139, U.S.A.

and S. SOMASEKHAR
Raman Research Institute, Bangalore 560 080, India

and R. SHASHIDHAR
Center for Bio/Molecular Science and Engineering, Code 6090, Naval Research Laboratory, Washington, D.C. 20375, U.S.A.

(*Received 20 July 1992; accepted 28 September 1992*)

The phase diagram has been established for binary mixtures of nonyloxybiphenyl cyanobenzoate (9OBCB) and pentylphenylcyanobenzoyloxy benzoate (DB_5CN). These frustrated liquid crystals exhibit a rich variety of polymorphic smectic A (S_A) and smectic C (S_C) phases. X-ray and calorimetric studies have been made of S_{A_d}–$S_{\tilde{C}}$–S_{C_2} and S_{A_d}–S_{A_1}–$S_{\tilde{C}}$–S_{A_2}–S_{C_2} phase sequences. Major emphasis is given to the tilted ribbon smectic ($S_{\tilde{C}}$)–bilayer smectic A (S_{A_2}) transition and the S_{A_2}–S_{C_2} transition. The former is first order, but there is substantial pretransitional heat capacity in the $S_{\tilde{C}}$ phase that can be described by an inverted Landau model. The latter transition is second order and exhibits a classical Landau step in C_p, in contrast to the behaviour of S_A–S_C transitions in non-polar systems where an extended Landau model with a large sixth order term is required.

1. Introduction

Liquid crystal molecules with strongly polar head groups and long (three-ring) aromatic cores are called frustrated smectics since there is a competition between two order parameters with incommensurate wave vectors [1]. Such compounds and their binary mixtures exhibit a large variety of smectic A (S_A) and smectic C (S_C) polymorphism [2]. The present paper reports the results of microscopic, X-ray, and calorimetric investigations of mixtures of nonyloxybiphenyl cyanobenzoate (9OBCB) and pentylphenylcyanobenzoyloxy benzoate (DB_5CN). The optical microscopy, the X-ray measurements, and a few differential scanning calorimetry (DSC) runs were made at the Raman Research Institute. High resolution AC calorimetric measurements were made at MIT.

The phase diagram for 9OBCB + DB_5CN is shown in figure 1. The various phases that appear are the isotropic, nematic, partial bilayer smectic A_d, monolayer smectic A_1, bilayer smectic A_2, tilted ribbon phase smectic C̃, and tilted bilayer smectic C_2. For smectic A phases with layer thickness d, $d \simeq L$ for S_{A_1}, $d \simeq 2L$ for S_{A_2}, and $L < d < 2L$ for

* Author for correspondence.

0267–8292/93 $10·00

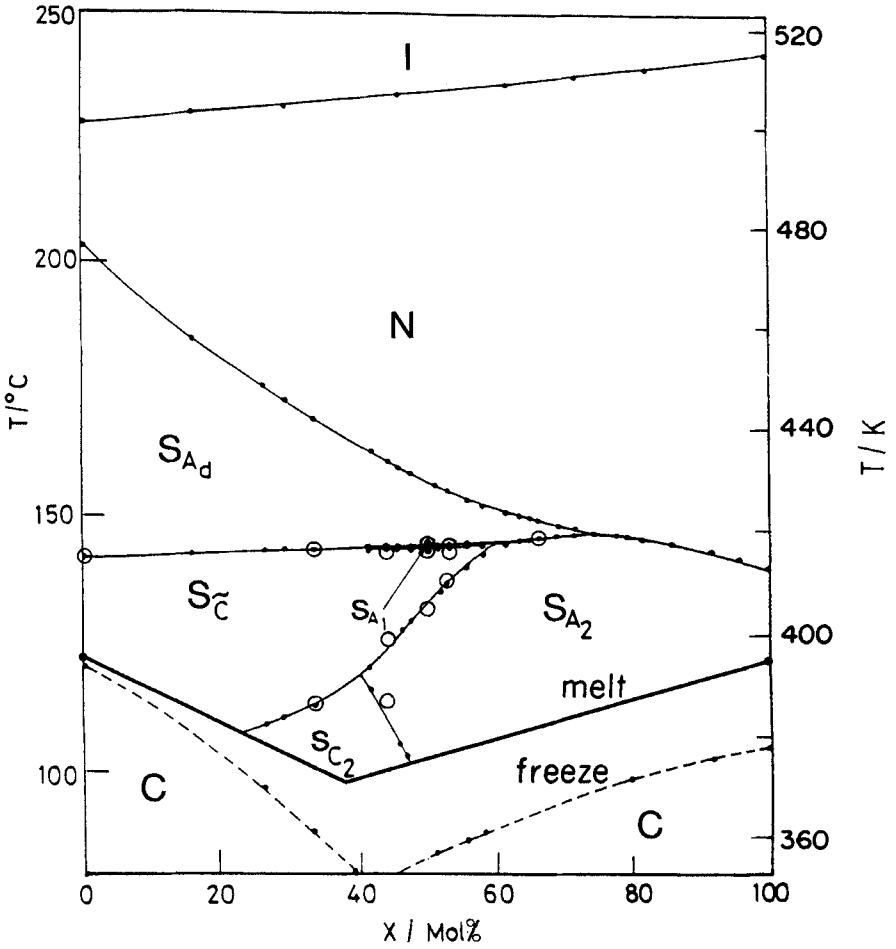

Figure 1. The phase diagram for 9OBCB + DB_5CN mixtures. Solid points were determined on cooling from optical textures; the open circles mark transition temperatures obtained from X-ray and calorimetric studies. The solid lines between the heavy dots at $X=0$ and $X=100$ sketch the temperatures at which crystal C melts on heating. The dashed lines indicate the non-equilibrium freezing temperatures of the monotropic smectic A_2, C_2, and $\tilde{C}$ phases on cooling a sample between microscope slides at the rate of 1 K min^{-1}. X is the mol% of DB_5CN.

S_{A_d}, where L denotes the average molecular length. Also shown in figure 1 are the freezing temperatures, where the crystal phase appears on cooling, and the melting temperatures. The principal goal of this work is to characterize the $S_{\tilde{C}}$–S_{C_2} and $S_{\tilde{C}}$–S_{A_2}–S_{C_2} phase sequences, but we also report briefly on the S_{A_d}–$S_{\tilde{C}}$, S_{A_d}–S_{A_1}–$S_{\tilde{C}}$, and S_{A_d}–S_{A_2} transitions. No studies have been made of the N–I, N–S_{A_d}, or N–S_{A_2} transitions.

2. Experimental results

The molecular formulae and molecular weights of the investigated compounds are

9OBCB ($M=441$ g)

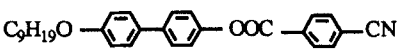

DB_5CN ($M = 413$ g)

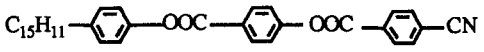

These compounds were synthesized and purified at the Raman Research Institute [3], and the phase diagram given in figure 1 was determined from a microscopic study of optical textures. Note the very narrow temperature and composition range over which a S_{A_1} phase is observed. Although not precisely determined, the estimated concentration limits for S_{A_1} are $42 < X < 58$, where X is the mol% of DB_5CN. The non-equilibrium freezing temperatures represent those observed for rapid cooling during the microscopic work and are sensitive to sample configuration and cooling rate. The melting lines determined calorimetrically are less well established but represent true thermodynamic transition temperatures. Various transition temperatures obtained from the X-ray data and high resolution calorimetry are in good agreement with the microscopic values, as shown in figure 1.

2.1. *Heat capacity data*

The temperature variation of C_p, the heat capacity per gram, was measured with a high resolution AC calorimeter, for which a detailed description has been given previously [4]. Measurements were made on samples with $X = 0$ (pure 9OBCB), 33, 41, 44 and 50. The sample with $X = 41$ showed rounded C_p peaks at the transitions and large drifts in transition temperatures T_0 with time (1–2·8 K day^{-1}). These $X = 41$ data agreed qualitatively with those from other samples, but they were not of sufficient quality to merit detailed analysis. All other samples were relatively stable, with T_0 drift rates of $-0{\cdot}06$ to $-0{\cdot}4$ K day^{-1} for the S_{A_d}–$S_{\tilde{C}}$ transition and $+0{\cdot}1$ to $0{\cdot}56$ K day^{-1} for $S_{\tilde{C}}$–S_{A_2} and $S_{\tilde{C}}$–S_{C_2} transitions.

Figure 2 shows the C_p behaviour at the S_{A_d}–$S_{\tilde{C}}$ transition for samples with $X = 0$ and $X = 44$. The transition is strongly first order in both these samples and in those with $X = 33$ and $X = 41$ (not shown). The width of the two phase coexistence range is 0·40 K for $X = 0$, 0·27 K for $X = 33$, 0·24 K for $X = 41$, and 0·70 K for $X = 44$. For the three samples with $X \leqslant 41$, there is no indication in the heat capacity data of a S_{A_1} phase. In the case of the $X = 44$ sample, two overlapping S_{A_d}–S_{A_1} and S_{A_1}–$S_{\tilde{C}}$ coexistence regions might possibly be hidden in the broad anomalous coexistence region for this sample. A DSC cooling scan carried out at $-0{\cdot}5$ K min^{-1} on this sample showed two distinct peaks 0·8 K apart, indicating a S_{A_1} phase over that narrow range. The presence of two closely-spaced transitions is clearly established by the AC calorimetric data for the $X = 50$ sample, as shown in figure 2. These S_{A_d}–S_{A_1} and S_{A_1}–$S_{\tilde{C}}$ transitions are 2·03 K apart and are first order with coexistence widths of 0·77 K and 0·19 K, respectively. Such coexistence widths are typical for these transitions [5]. DSC data for a mixture with $X = 65{\cdot}6$ show a single sharp (first order) S_{A_d}–S_{A_2} peak at 419·7 K; no AC calorimetric measurements were made on this transition.

The transitions observed on cooling the $S_{\tilde{C}}$ phase are shown in figure 3. For $X = 33$, there is a direct and strongly first order transition from $S_{\tilde{C}}$ to S_{C_2}. Data points between the pair of vertical lines represent artificial C_p values obtained in a two-phase coexistence region. The phase shift ϕ between the oscillating heat input $Q(\omega)$ and the sample temperature $T(\omega)$ displays an abrupt anomalous increase when two phases coexist [4], and this is an additional indication of a first order transition. $S_{\tilde{C}}$–S_{A_2} transitions, also first order but with substantial pretransitional C_p above the transition, were observed for mixtures with $X = 44$ and 50. A second order S_{A_2}–S_{C_2} transition was observed for $X = 44$ but not for $X = 50$ since that mixture froze at 367 K (above the S_{A_2}–S_{C_2} transition temperature). Fits to the $S_{\tilde{C}}$–S_{A_2} and S_{A_2}–S_{C_2} data are discussed later.

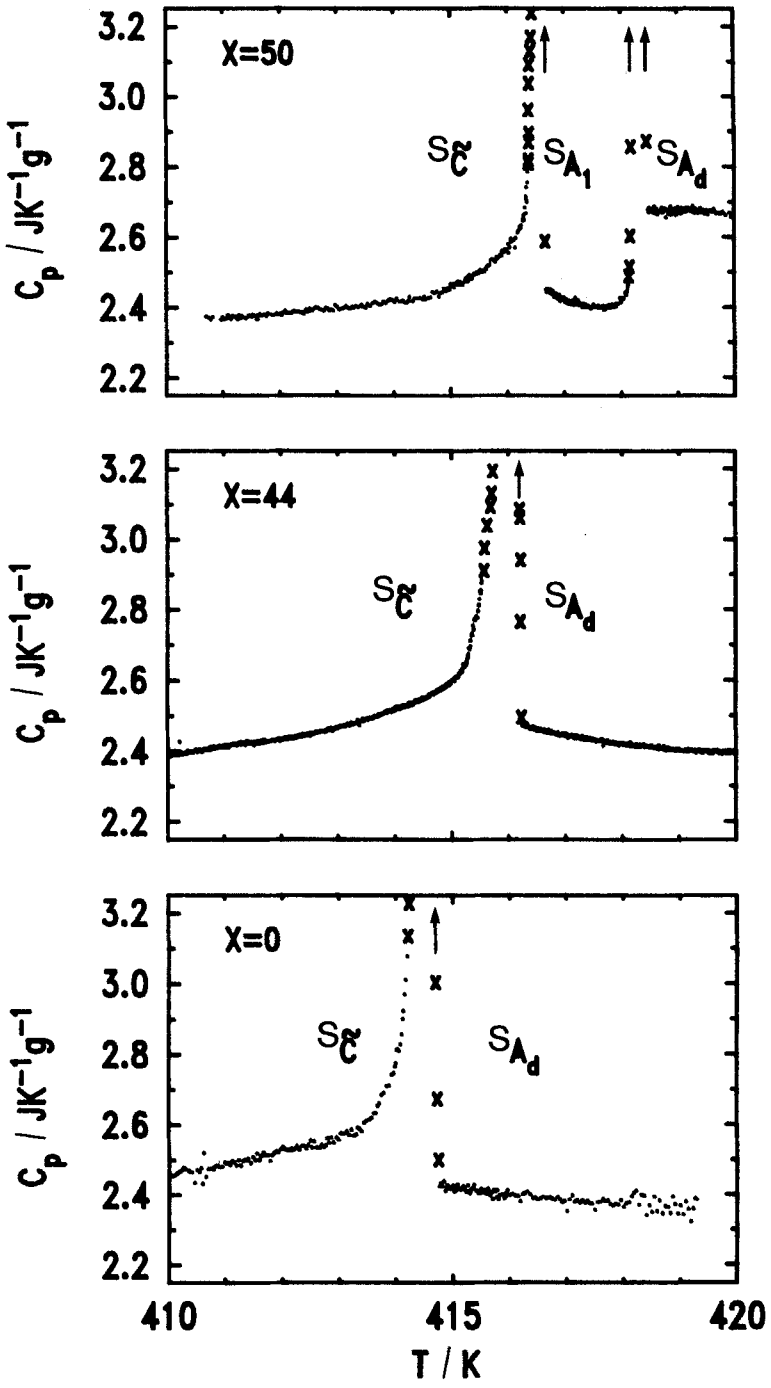

Figure 2. The heat capacity near the S_{A_d}–$S_{\tilde{C}}$ transition in pure 9OBCB and a 9OBCB + DB_5CN mixture with $X = 44$. Also given is the C_p variation through the S_{A_d}–S_{A_1}–$S_{\tilde{C}}$ sequence in a sample with $X = 50$. Points denoted by × are anomalous C_p values in a two-phase coexistence region; many of these lie off scale.

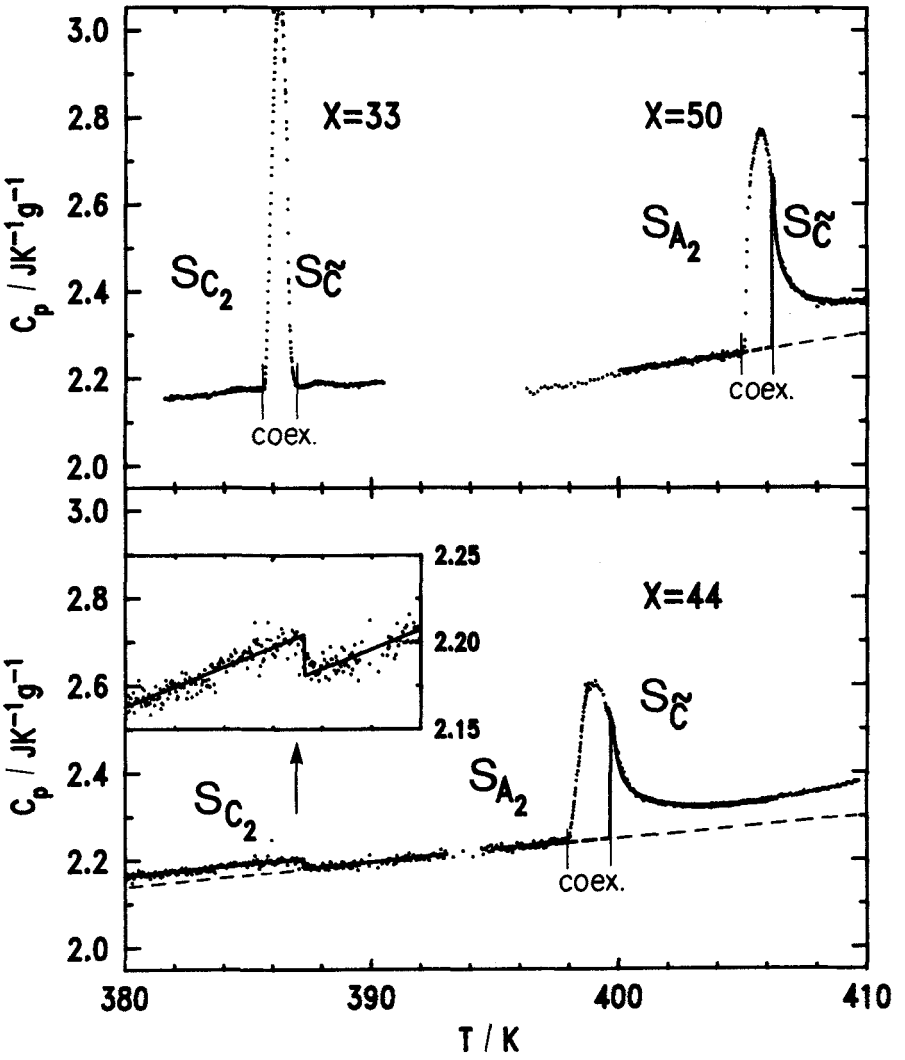

Figure 3. The heat capacity variation near the lower temperature transitions at which the $S_{\tilde{C}}$ phase transforms into S_{A_2} or S_{C_2} phase. Points between the vertical lines are anomalous C_p values in a two-phase coexistence region. The smooth curves represent inverted Landau fits to the $S_{\tilde{C}}$–S_{A_2} transitions with equation (1) and a classic Landau fit to the S_{A_2}–S_{C_2} data with equation (2).

2.2. *X-ray data*

Measurements were made with an X-ray set-up utilizing photographic detection of the scattering. The nickel filtered radiation was focused on the sample using a bent quartz monochrometer. Samples were contained in 0·5 mm Lindemann capillaries and aligned in the nematic phase with a 4 kG magnet. Further details are given elsewhere [6].

A sample with $X = 52{\cdot}6$ exhibits the phase sequence S_{A_d}–S_{A_1}–$S_{\tilde{C}}$–S_{A_2} and the observed temperature dependence of the scattering wave vectors is given in figure 4. In the S_{A_d} phase, the scattering consists of a pair of quasi-Bragg condensed spots at $(0, 0, \pm q_0')$, where $q_0' = 2\pi/d$. On cooling, q_0' decreases from 0·1355 Å^{-1} at 421·7 K to 0·131 Å^{-1} at 416·95 K (the S_{A_d}–S_{A_1} transition), i.e. $d(T)$ increases from 46·4 Å to 48·0 Å.

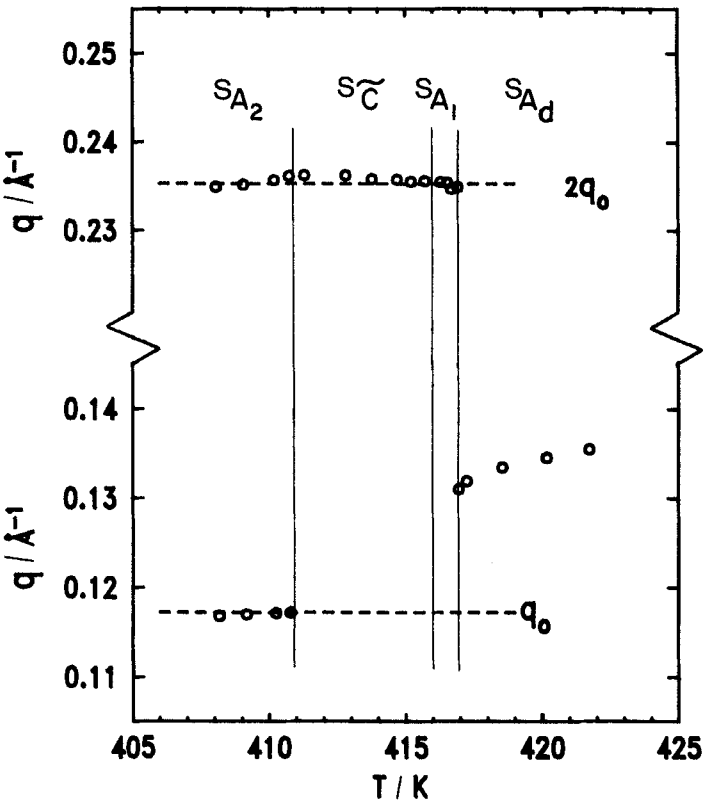

Figure 4. The variations of the scattering wave vectors with temperature for a 9OBCB + DB_5CN mixture with $X = 52{\cdot}6$. The $S_{\tilde{C}}$ data are distinguishable from S_{A_1} data due to the presence (not shown) of off-axis peaks associated with the in-plane polarization modulation.

In the S_{A_1} phase, the diffraction spots occur at $(0, 0, \pm 2q_0)$, where $2q_0 = 2\pi/L = 0{\cdot}235$ Å^{-1}. This yields a temperature-independent S_{A_1} layer thickness of 26·75 Å over the range 416–416·95 K. In the $S_{\tilde{C}}$ phase, there are $(0, 0, \pm 2q_0)$ spots plus two pairs of off-axis spots of unequal intensity, a clear indication of the $S_{\tilde{C}}$ ribbon phase [7]. The temperature-independent value of $2q_0$ in the $S_{\tilde{C}}$ phase is 0·236 Å^{-1}, which yields a layer thickness of 26·65 Å. Finally, at temperatures below 411 K the scattering is characteristic of the S_{A_2} phase—a pair of spots at $(0, 0, \pm q_0)$ as well as the pair at $(0, 0, \pm 2q_0)$. The observed wave vectors are $q_0 = 0{\cdot}1175$ Å^{-1} and $2q_0 = 0{\cdot}235$ Å^{-1}, corresponding to a bilayer thickness of 53·5 Å. X-ray measurements on a sample with $X = 65{\cdot}6$ (not shown) exhibit a strong first order S_{A_d}–S_{A_2} transition. This transition at 419·5 K with a 0·3 K wide coexistence region involves a discontinuous jump in d from 49·0 Å (S_{A_d}) to 51·5 Å (S_{A_2}).

3. Discussion

The X-ray data in figure 4 show that there is essentially no tilt in the director with respect to the layer normal in this $S_{\tilde{C}}$ phase. Thus the mass density ordering is almost the same as that in a smectic A phase, and it is the lateral polarization modulation that is tilted. In essence, the oblique centred $S_{\tilde{C}}$ lattice is a polarization sheared variant of the antiphase $S_{\tilde{A}}$ structure; see figure 10 in [5].

It follows that the $S_{\tilde{C}}$–S_{A_2}–S_{C_2} phase transition sequence in 9OBCB + DB_5CN is very closely related to the $S_{\tilde{C}}$–S_{C_2} transition observed in $DB_8ONO_2 + DB_{10}ONO_2$ mixtures, where DB_nONO_2 is alkyloxyphenyl-nitrobenzoyloxy benzoate [5]. In particular, the $S_{\tilde{C}}$–S_{A_2} heat capacity behaviour should be well described by a first order inverted Landau form given by [5]

$$C_p^- = C_p^0(T), \qquad T < T_1, \tag{1a}$$

$$C_p^+ = C_p^0(T) + A^*(T - T_k)^{-1/2}, \quad T > T_1, \tag{1b}$$

where $C_p^0(T)$ is the regular background heat capacity variation and T_1 is the first order transition temperature. Fits to the $S_{\tilde{C}}$–S_{A_2} data for $X = 44$ and $X = 50$ are shown in figure 3, and the fitting parameters are given in the table. Pseudo C_p values in the coexistence region are not represented by equation (1) and are not included in these fits. The choice of T_1 is somewhat arbitrary, but it must be located somewhere in the coexistence region. The temperature T_k represents the metastability limit for this inverted Landau model [5]. It should be noted that the anomalous C_p behaviour in the $S_{\tilde{C}}$–S_{A_2} coexistence region is very similar to the C_p behaviour reported [8] in the $S_{A_{cren}}$ crenelated phase (which occurs between the fluid antiphase $S_{\tilde{A}}$ and S_{A_2} and has a special character much like two phase coexistence).

The $C_p(S_{A_2}$–$S_{C_2})$ variation in other polar bilayer systems [9, 10] is well described by the classic second order Landau form

$$\Delta C_p = 0, \qquad T > T_c, \tag{2a}$$

$$\Delta C_p = A(T/T_c) \simeq A, \quad T < T_c, \tag{2b}$$

where $\Delta C_p = C_p(S_{C_2}) - C_p^0(T)$. The best fit to the S_{A_2}–S_{C_2} behaviour for the $X = 44$ sample with equation (2) is shown in figure 3. The values of the fitting parameters are $A = 0{\cdot}024\ J\,K^{-1}\,g^{-1}$ and $T_c = 387{\cdot}3 \pm 0{\cdot}2$ K. In order to compare the size of this C_p step with those in other systems, it is useful to transform A into a dimensionless quantity $A_R \equiv AM/R$. Using an average molecular weight of 428·7 g for this $X = 44$ sample, we obtain $A_R = 1{\cdot}23$, which is quite small. The other known A_R values for S_{A_2}–S_{C_2} transitions are 4·8 in heptyloxycarbonylphenylcyano-benzoyloxy benzoate (7APCBB) [10] and 32·7 in octylphenyl-chlorocyanobenzoyloxy benzoate (DB_8CICN) [9]. It should be stressed that S_{A_2}–S_{C_2} transitions require a Landau model with a very small or zero sixth order coefficient in the free energy, whereas S_A–S_C transitions in non-polar liquid crystals all require an extended Landau model with a large sixth order coefficient. (See [9, 10] for further discussion of this issue.) Since the S_{A_2}–S_{C_2} transition line is a second order line that terminates at the first order melting line and at the first

Least-squares values of the parameters in equation (1) obtained on fitting $S_{\tilde{C}}$–S_{A_2} heat capacity data in 9OBCB + DB_5CN mixtures. The background curves $C_p^0(T)$ are given by the dashed lines in figure 3. The units for A^* are $J\,K^{-1/2}\,g^{-1}$. Comparable parameters for the $S_{\tilde{C}}$–S_{C_2} transition in a DB_nONO_2 mixture [4] are given for comparison.

X	T_1/K	T_k/K	A^*	χ_ν^2
44	~399·7	399·633	0·42	1·09
50	~406·2	406·152	0·55	1·07
51·33	372·67	372·629	0·265	0·98
$DB_8ONO + DB_{10}ONO_2$				

order transition line into the $S_{\tilde{C}}$ phase, two critical end points are implied. However, there are insufficient S_{A_2}–S_{C_2} data to characterize this line in greater detail.

In conclusion, it should be noted that the inverted Landau behaviour for $S_{\tilde{C}}$–S_{A_2} transitions and the step-like classic Landau behaviour for the S_{A_2}–S_{C_2} transition confirm and support the analysis given previously for the $S_{\tilde{C}}$–S_{C_2} in DB_8ONO_2 + $DB_{10}ONO_2$ mixtures [5].

The work at MIT was supported by National Science Foundation grant DMR 90-07611.

References

[1] PROST, J., and BAROIS, P., 1983, *J. Chim. phys.*, **80**, 65. PROST, J., 1984, *Adv. Phys.*, **33**, 1.
[2] HARDOUIN, F., LEVELUT, A. M., ACHARD, F., and SIGAUD, G., 1983, *J. Chim. Phys.*, **80**, 53. GARLAND, C. W., 1990, *Geometry and Thermodynamics: Incommensurate Crystals, Liquid Crystals, and Quasicrystals*, edited by J. C. Toledano (NATO ASI Ser. B) (Plenum), pp. 221–254 and references cited therein.
[3] The synthetic procedures used for 9OBCB were those given in GOODBY, J. W., and WALTON, C. R., 1985, *Molec. Crystals liq. Crystals*, **122**, 219. See also CLADIS, P. E., and BRAND, H. R., 1984, *Phys. Rev. Lett.*, **52**, 2261. The procedures used to synthesize DB_5CN were those given in: TINH, N. H., 1983, *J. Chim. phys.*, **80**, 83.
[4] GARLAND, C. W., 1985, *Thermochim. Acta*, **88**, 127.
[5] EMA, K., NOUNESIS, G., GARLAND, C. W., and SHASHIDHAR, R., 1989, *Phys. Rev.* A, **39**, 2599.
[6] RATNA, B. R., KRISHNA PRASAD, S., SHASHIDHAR, R., HEPPKE, G., and PFEIFFER, S., 1985, *Molec. Crystals liq. Crystals*, **124**, 21.
[7] HARDOUIN, F., TINH, N. H., ACHARD, M. F., and LEVELUT, A. M., 1982, *J. Phys. Lett., Paris*, **43**, L-327. SAFINYA, C. R., VARADY, W. A., CHIANG, L. Y., and DIMON, P., 1986, *Phys. Rev. Lett.*, **57**, 432.
[8] EMA, K., GARLAND, C. W., SIGAUD, G., and NGUYEN HUU TINH, 1989, *Phys. Rev.* A, **39**, 1369, see figure 9 therein.
[9] JEONG, Y. H., STINE, K. J., GARLAND, C. W., and TINH, N. H., 1988, *Phys. Rev.* A, **37**, 3465.
[10] WEN, X., GARLAND, C. W., and HEPPKE, G., 1991, *Phys. Rev.* A, **44**, 5064.